ACS OMEGA

Article

Cite This: ACS Omega 2018, 3, 5459−5469

In Vitro Carcinoma Treatment Using Magnetic Nanocarriers under Ultrasound and Magnetic Fields

Somoshree Sengupta,[†,‡] Chandra Khatua,[†,‡] and Vamsi K. Balla*[,†,‡]

[†]Bioceramics & Coating Division, CSIR-Central Glass & Ceramic Research Institute, 196 Raja S.C. Mullick Road, Kolkata 700032, India

[‡]Academy of Scientific and Innovative Research (AcSIR), CSIR-Central Glass & Ceramic Research Institute Campus, 196 Raja S.C. Mullick Road, Kolkata 700032, India

ABSTRACT: Nowadays, tumor hypoxia has become a more predominant problem for diagnosis as well as treatment of cancer due to difficulties in delivering chemotherapeutic drugs and their carriers to these regions with reduced vasculature and oxygen supply. In such cases, external physical stimulus-mediated drug delivery, such as ultrasound and magnetic fields, would be effective. In this work, the effect of simultaneous exposure of low-intensity pulsed ultrasound and static magnetic field on colon (HCT116) and hepatocellular (HepG2) carcinoma cell inhibition was assessed in vitro. The treatment, in the presence of anticancer drug, with and without magnetic carrier, significantly increased the reactive oxygen species production and hyperpolarized the cancer cells. As a result, a significant increase in cell inhibition, up to 86%, was observed compared to 50% inhibition with bare anticancer drug. The treatment appears to have relatively more effect on HepG2 cells during the initial 24 h than on HCT116 cells. The proposed treatment was also found to reduce cancer cell necrosis and did not show any inhibitory effect on healthy cells (MC3T3). Our in vitro results suggest that this approach has strong application potential to treat cancer at lower drug dosage to achieve similar inhibition and can reduce health risks associated with drugs.

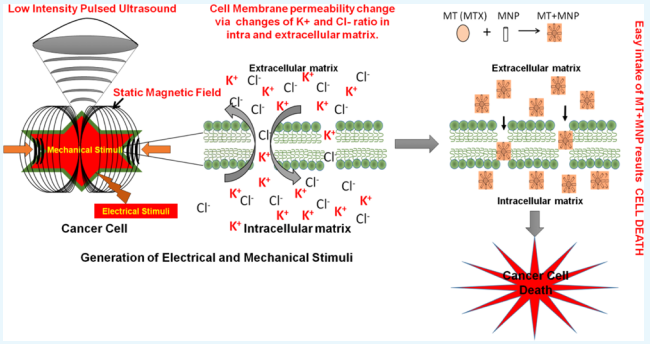

1. INTRODUCTION

In general, around the tumor environment, highly proliferating mass of cells cause oxygen deficiency,[1] leading to the formation of hypoxic zones, which are difficult to penetrate by the standard chemotherapeutic or anticancer drugs due to reduced vascular structure.[2] Similarly, radiotherapy is also ineffective to treat tumors with deoxygenated regions, as molecular oxygen is essential to achieve the desired biological effect of ionizing radiation on cancer.[3] Hypoxia is also known to effect tumor cell division and invasion (autonomous functions) and non-autonomous processes, such as angiogenesis, lymph angiogenesis, and inflammation, which are observed during metastasis.[4] Therefore, researchers developed a magnetic field-assisted treatment, where the drug-loaded vehicles are guided and delivered to the hypoxic regions of the tumor using external magnetic fields. External magnetic fields are also being used to trigger the release of drug from the magnetic carrier at the tumor site.[5] Surface-modified microbubbles, triggered by external ultrasound (US), have also been used to treat the hypoxic zone of human breast cancer. The potential application of such ultrasound-triggered oxygen delivery to solid tumors improved the condition of tumor within 30 days.[6] The potential of this approach in targeting brain tumor using magnetic drug carriers has also been demonstrated.[7,8] Magnetic nanoparticles (MNP) have been extensively used for various biomedical applications including cancer.[8] Ferromagnetic nanoparticles (NPs) become magnetized under externally applied magnetic fields and can easily agglomerate even in the absence of magnetic fields. However, the use of paramagnetic or weakly ferromagnetic NPs can eliminate this problem as they do not exhibit magnetization in the absence of externally applied magnetic fields.[9] Therefore, paramagnetic or weakly ferromagnetic NPs can be easily dispersed by magnetic field for uptake of phagocytes and increasing their half-life in the circulation.[10]

An important variant of magnetic field-based cancer treatment involves hyperthermia using MNP,[11] where extreme temperature elevation in the tumor cells (>40 °C) leads to denaturation of the cellular protein and cellular death. However, the use of MNP as drug-delivery system (DDS) is associated with issues such as difficulties in measuring dose concentration, dose dumping, and restricted range of hyperthermia.[12] Accumulation of MNP also effects their biological response as DDS leads to rapid clearance of MNP from cells;[13] therefore, high concentration of MNP is required to achieve the desired therapeutic outcome. According to the literature, minimum concentration of MNP required for effective

Received: January 17, 2018
Accepted: May 7, 2018
Published: May 21, 2018

DOI: 10.1021/acsomega.8b00105
ACS Omega 2018, 3, 5459−5469

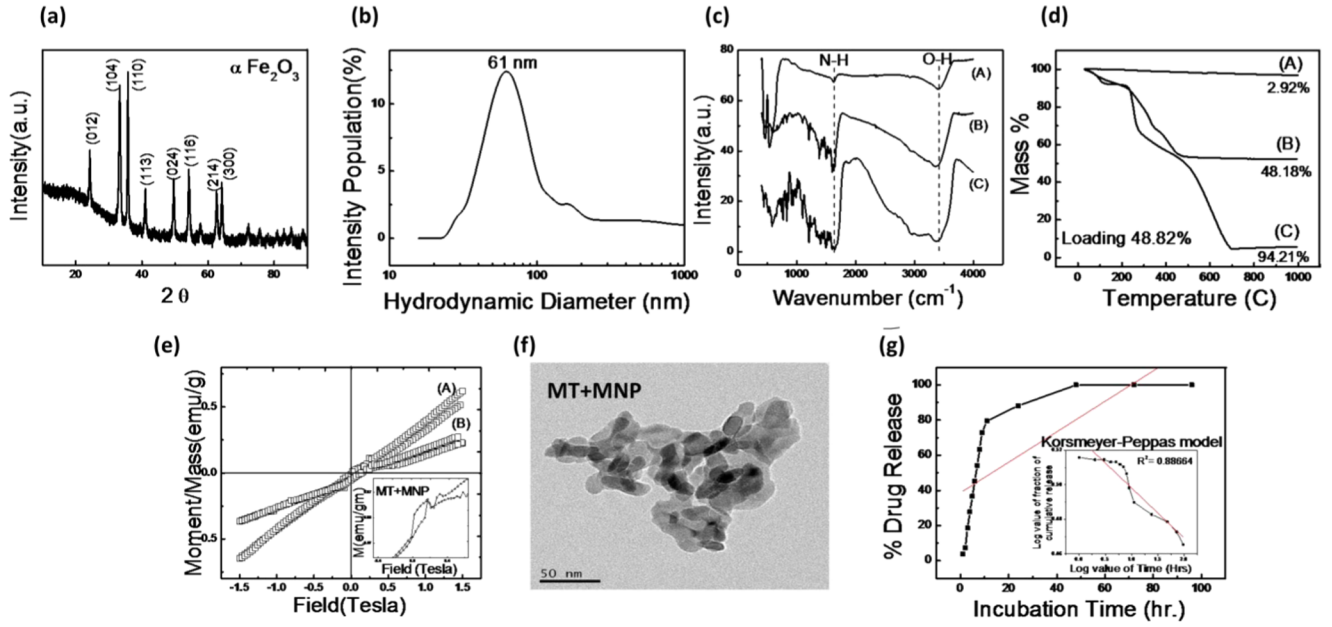

Figure 1. (a) XRD analysis of MNP after calcination at 450 °C for 2 h. (b) Particle size analysis of MT + MNP. (c) FTIR spectra of (A) MNP (α-Fe_2O_3), (B) MT + MNP (MT + α-Fe_2O_3), and (C) MT. (d) Thermogravimetric (TG) analysis (TGA) of (A) MNP, (B) MT + MNP, and (C) MT. (e) Magnetic properties of (A) MNP and (B) MT + MNP. (f) Transmission electron microscopy analysis of MT + MNP. (g) Release of MT from MT + MNP in phosphate-buffered saline (PBS, pH 7.4).

hyperthermia is between 1 and 2 mol/kg body mass, which is significantly higher than the concentration required for magnetic resonance imaging and can effect nearby healthy tissues.[14] More importantly, after repeated hyperthermia, the cells were found to exhibit thermoresistance again and therefore the treatment efficacy decreases.[15] On the other hand, external magnetic fields have been used to avoid agglomeration and accumulation of MNP, which can lead to local toxicity.[16]

In general, the use of static magnetic fields (SMF) as adjuvant therapy toward cancer treatment has shown some promising results in animal studies.[17−20] SMF increased the oxidative stress leading to cellular membrane damage and apoptosis in cancer cells.[21] Moreover, the interaction between the SMF (200−2000 mT) and polar, ionic molecules of the cancer cellular compartment can also generate reactive oxygen species (ROS)[22] and thus inhibit their growth. ROS production[23] is also found to damage the ion channels of cancer cells, leading to changes in their morphology and apoptosis. The application of SMF along with anticancer drug improved the drug efficacy and can eliminate the probability of scar formation and infection.[24] In myelogenous leukemia (K562) cells, the use of 8.8 mT SMF effectively enhanced the potencies of various drugs (cisplatin, taxol, doxorubicin (DOX), and cyclophosphamide).[25] Large apophyses of 0.47 μm diameter and irregular apophyses (1.85 and 2.04 μm in diameter) were formed with SMF application, which triggered the uptake of anticancer drug and enhanced the potency of these drugs.[26] It appears that the use of SMF is effective in addressing the thermoresistance of cancer cells to repeated hyperthermia and high concentration of MNP required to create effective hyperthermia.

Another important noninvasive cancer treatment approach is ultrasound (US)-mediated targeted drug delivery,[27] which depends on mechanical effects to induce stress response and apoptosis in several cancer cell lines.[28−31] US-assisted cancer treatment effectively enhanced cancer cell inhibition or death in the presence of drugs and DDS.[32−36] Typically, US creates acoustic waves within the biological soft tissues through nonthermal physical mechanisms that produce molecular vibration in the tissue, resulting in mechanical stimulation to accelerate membrane potential changes.[37] Among different types of US, low-intensity pulsed ultrasound (LIPUS) was found to alter cellular membrane properties in damaged or diseased cells without effecting the normal cells.[38] Human uterine sarcoma cell line (FU-MMT-3) treated with LIPUS (1 MHz, 2 W/cm^2, 50% duty cycle, 60 s) in the presence of irinotecan (CPT-11) and SN38[38] showed VEGF inhibition. Similarly, the effectiveness of doxorubicin (DOX) on human primary liver cancer cells has been enhanced with the application of LIPUS.[39]

Nonetheless, the concept of utilizing SMF along with LIPUS to facilitate enhanced drug delivery is not reported yet. In this investigation, we have examined the use of SMF in the presence of LIPUS, which can create Lorentz force on the cells/tissues,[22] that rapidly oscillates the cells/ions/tissue and generates local electrical currents/fields.[22] Since the endogenous electrical fields, present in the extracellular milieu, influence the cell behavior,[40] the SMF + LIPUS-generated in situ fields can also influence cellular membrane, nucleus,[41] etc. Some investigators demonstrated the effectiveness of externally applied electrical fields in treating melanomas,[42] enhanced drug inhibitory effects[43] and tumors.[44] Therefore, it is believed that the electrical fields generated in situ with the combined use of SMF and LIPUS can influence cancer cell activities and that the mechanical stress generated due to LIPUS might also have a synergetic role. In this investigation, we have focused to evaluate the influence of LIPUS + SMF treatment on cancer cell inhibition in the presence of MNP with anticancer drugs. We have also made an attempt to understand the response of two different cancer cells to this external treatment.

DOI: 10.1021/acsomega.8b00105
ACS Omega 2018, 3, 5459−5469

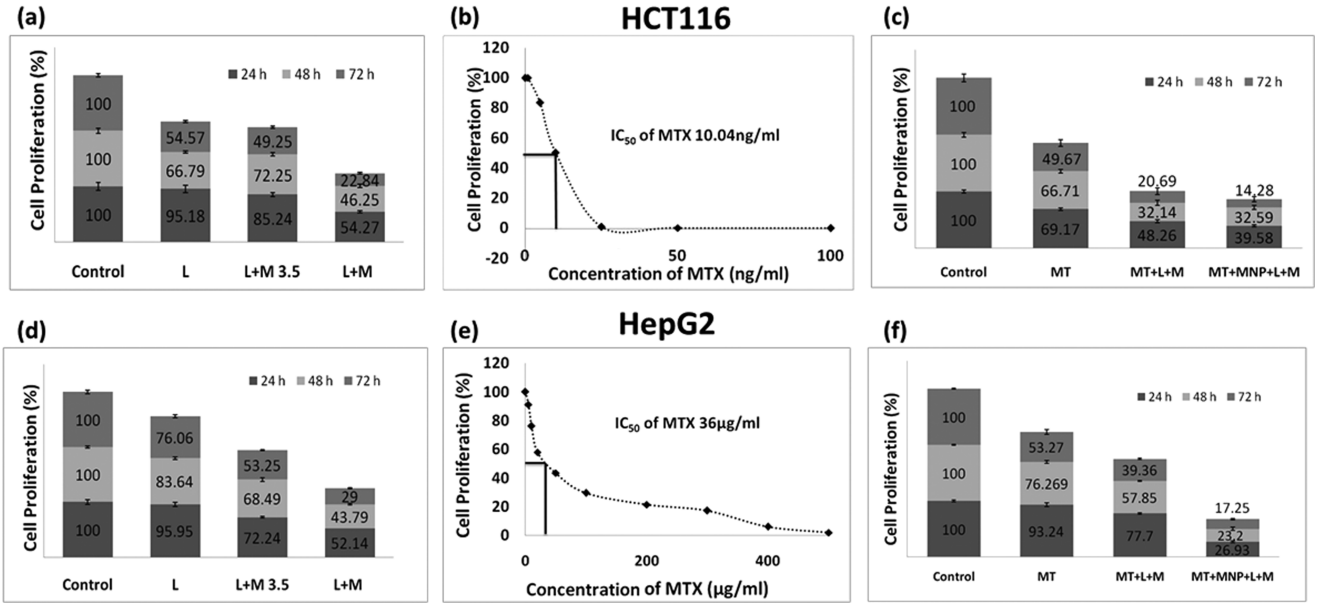

Figure 2. (a) HCT116 cell proliferation under 15 min/day treatment of 30 mW/cm^2 LIPUS (L), 3.5 mT SMF (L + M3.5), and 30 mW/cm^2 LIPUS + 150 mT SMF (L + M) ($p < 0.05$ between control and treated samples) ($n = 12$). (b) Dose response curve of MT on HCT116 cell viability and determination of IC_{50} ($n = 3$). (c) HCT116 cell proliferation under 15 min/day treatment of L + M when the cells were exposed to MT and MT + MNP ($p < 0.05$ between control and treated samples) ($n = 12$). (d) Proliferation assay of HepG2 cells under 15 min/day treatment of L + M3.5 and L + M ($p < 0.05$ between control and treated samples) ($n = 12$). (e) Dose response curve of MT on HepG2 cell viability and determination of IC_{50} ($n = 3$). (f) Proliferation assay of HepG2 under 15 min/day treatment of L + M when the cells were exposed to MT and MT + MNP ($p < 0.05$ between control and treated samples) ($n = 12$).

2. RESULTS

2.1. Characteristics of MNP and Methotrexate (MT) + MNP. The X-ray diffraction (XRD) analysis of MNP, presented in Figure 1a, revealed all peaks corresponding to α-Fe_2O_3 (JCPDS no. 24-0072). No other phases were observed in the calcined MNP. The crystallite size of the MNP calculated using the Scherrer formula was 25 nm, while the particle size of MT + MNP determined using the dynamic laser scattering technique was found to be 61 nm (Figure 1b). The ζ potential of MT + MNP was 50 mV, which signifies its stability in suspension for use as DDS. From the Fourier transform infrared (FTIR) spectra, two broad peaks at 555 and 463 cm^{-1} were identified for MNP (Figure 1c-A), which correspond to Fe−O stretching and bending vibration modes of α-Fe_2O_3, respectively.[45] The presence of a band at 1663 cm^{-1} is attributed to C═O double bond and C−O stretching vibration.[46] The absorption band of MT + MNP at 1385 cm^{-1} (Figure 1c-B) indicates high intensity of nitrate (NO_3^-) anions in their structure, which is an indication of MT adsorption on the surface of MNP. This is further corroborated by the absorption band in the broad range of 3400 cm^{-1}, which can be due to the stretching vibration of structural hydroxyl groups of surface-adsorbed water on MT + MNP.

During thermogravimetric analysis, the mass loss up to 250 °C in MT + MNP (Figure 1d-B) was due to the removal of loosely bound water from the powder. The decomposition between 220 and 400 °C was attributed to the decomposition of adsorbed nitrate ions from MT and dehydroxylation of the powder. The total mass loss of MNP was very low, up to 1000 °C (2.92%, Figure 1d-A). In the case of MT + MNP, it was 51.82% (Figure 1d-B), in which the initial mass loss, until 425 °C, was because of the water molecules of MNP. On the basis of thermogravimetric analysis, the immobilization of MT on MNP was estimated to be 48.82%. The magnetic behaviors of MNP and MT + MNP, shown in Figure 1e-A,e-B, respectively, demonstrate that both MNP samples exhibit weak ferromagnetic behavior with a slight paramagnetic behavior. The saturation magnetization of MNP was found to be higher (0.62 emu/g) than that of MT + MNP with a saturation magnetization of 0.27 emu/g. The decrease in the magnetization of MT + MNP could be due to the adsorption of a large amount (48.82%) of MT on its surface. The presence of diamagnetic coating or material on MNP can decrease the magnetic moment and therefore result in low magnetization.[47−49]

As shown in Figure 1f, the MT + MNP powder appears to have an average size of ∼50 nm. Figure 1g shows cumulative release of MT from MT + MNP in PBS at pH 7.4. The initial burst release of 80 wt % of MT during 8 h incubation was due to desorption of the strained MTX molecule bound to MNP. Cumulative release kinetics of MT from MNP was fitted into the Korsmeyer−Peppas model,[50] following $X = k(t - \alpha)^n$, where X, t, k, α, and n are the drug release (%), release time, kinetics constant, modified parameter, and an exponent, respectively.[50] The exponent n (apparently R^2) is normally used to describe different release mechanisms. The value of exponent n was estimated to be 0.88, which indicates that the release behavior of MT from MT + MNP is predominantly diffusion-controlled.

2.2. Influence of LIPUS + SMF Treatment on Cancer Cell Proliferation. Initially, proliferation of HCT116 and HepG2 cells was assessed using 30 mW/cm^2 LIPUS and its combination with 3.5 and 150 mT SMF, and the results are presented in Figure 2a,d, respectively. The proliferation of HCT116 cells marginally reduced when exposed to LIPUS during the first 24 h (Figure 2a) and the cell proliferation decreased at later culture durations. A significant amount of cell inhibition was observed when LIPUS was used in the presence

DOI: 10.1021/acsomega.8b00105
ACS Omega 2018, 3, 5459−5469

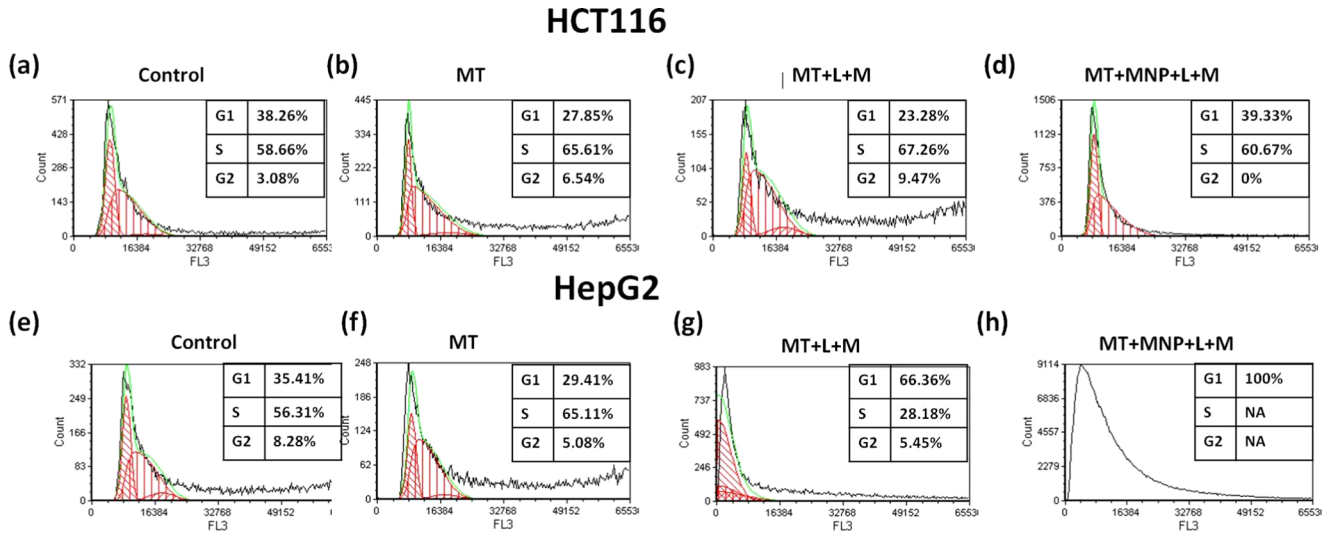

Figure 3. (a–d) Gated HCT116 cell population in different phases after 72 h of incubation (n = 6): (a) control (without MT); (b) MT-treated; (c) MT + L + M-treated; and (d) MT + MNP + L + M-treated. (e–h) HepG2 cell-cycle assessment showing gated cell population in different phases after 72 h incubation (n = 6): (e) control (without MT); (f) MT-treated; (g) MT + L + M-treated; and (h) MT + MNP + L + M-treated.

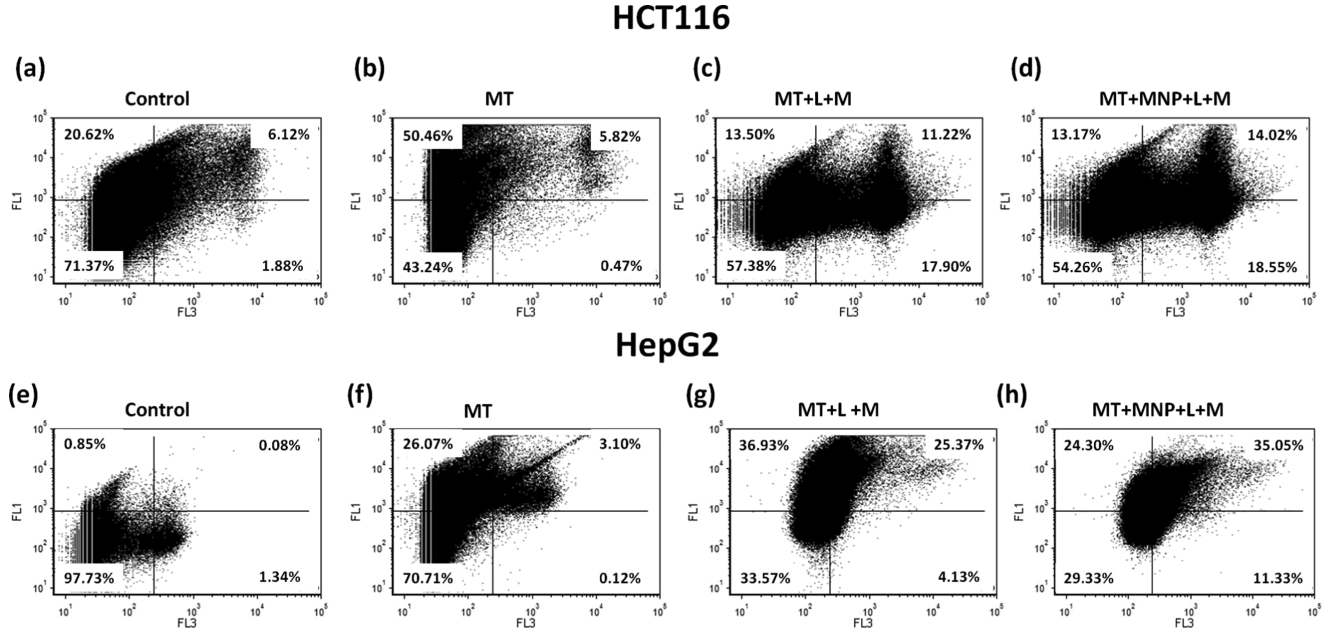

Figure 4. (a–d) Apoptosis analysis of HCT116 cells after 72 h incubation (n = 6): (a) control (without MT); (b) MT-treated; (c) MT + L + M-treated; and (d) MT + MNP + L + M-treated. (e–h) Apoptosis of HepG2 cells after 72 h incubation (n = 6): (e) control (without MT); (f) MT-treated; (g) MT + L + M-treated; and (h) MT + MNP + L + M-treated.

of 3.5 mT SMF (L + M3.5) at all culture durations, and with 150 mT SMF (L + M), further inhibition in HCT116 cells was achieved. Almost 80% cell inhibition was observed after 72 h of incubation with L + M, as shown in Figure 2a. A similar inhibition was exhibited by HepG2 cells under these treatment conditions (Figure 2d). The LIPUS treatment resulted in 5–20% inhibition in these cells, which was increased to 50 and 70% in the presence of 3.5 mT SMF (L + M3.5) and 150 mT SMF (L + M) at 72 h culture duration, respectively. Since both cell lines (HCT116 and HepG2) showed maximum inhibition with L + M treatment (30 mW/cm^2 LIPUS + 150 mT SMF), more detailed experiments were performed using this treatment. The influence of MT concentration on the viability of HCT116 and HepG2 cells is shown in Figure 2b,e, respectively. Form these dose response curves, the half-maximal inhibitory concentration (IC_{50}) concentration of MT was determined to be 10.04 ng/mL for HCT116 cells (Figure 2b) and 36 μg/mL for HepG2 cells (Figure 2e). Further experiments in the presence of MT drug were carried out using the IC_{50} concentration of respective cell lines.

The influence of different treatment conditions on the proliferation of HCT116 cells is shown in Figure 2c. The cell proliferation decreased with culture duration under all treatment conditions. However, the severity of cell inhibition was highest with MT + MNP + L + M treatment. During the initial 24 h, the inhibition of HCT116 cells was 30% with the bare drug (MT), which increased to 50% with L + M treatment (MT + L + M). Further enhancement in the cellular inhibition

DOI: 10.1021/acsomega.8b00105
ACS Omega 2018, 3, 5459–5469

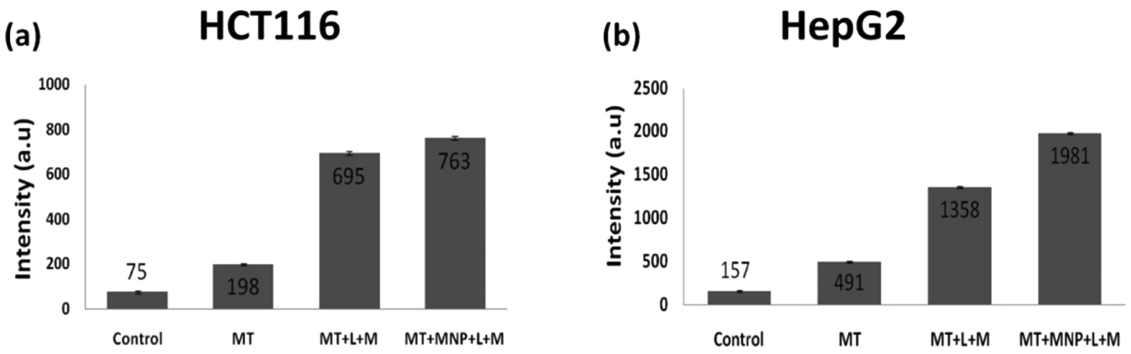

Figure 5. Measured intracellular ROS in terms of fluorescence intensity. (a) HCT116 cells treated with MT, MT + L + M, and MT + MNP + L + M. (b) HepG2 cells treated with MT, MT + L + M, and MT + MNP + L + M. The control group had no treatment.

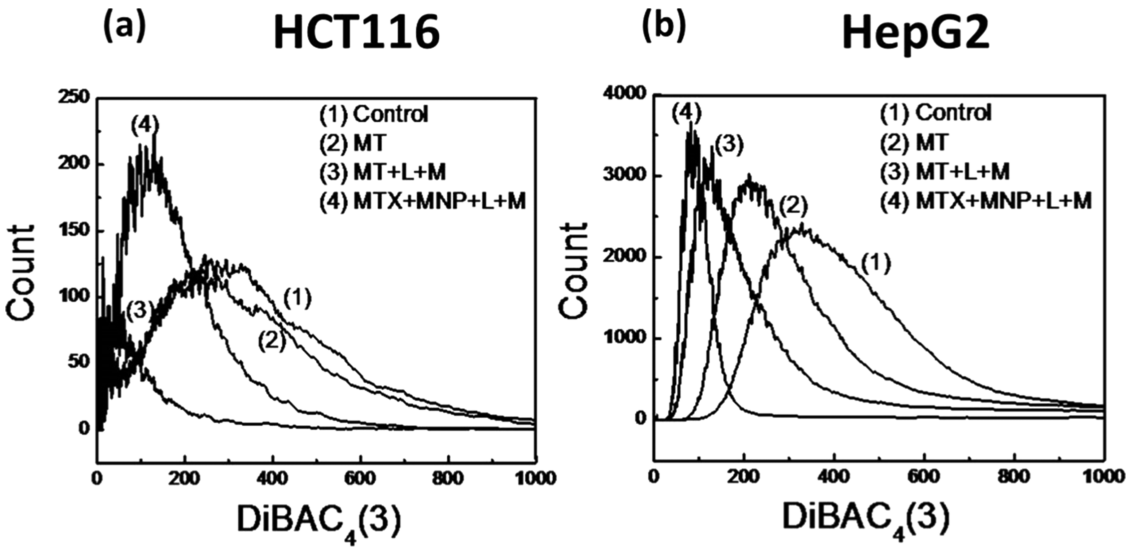

Figure 6. Changes in the membrane potential determined using voltage-sensitive bis(1,3-dibutylbarbituric acid)trimethineoxonol ($DiBAC_4(3)$) dye (n = 6): (a) HCT116 cells and (b) HepG2 cells.

(60%) was achieved with MT + MNP + L + M, where the drug was delivered using MNP. After 72 h of culture, the MT + MNP + L + M treatment restricted the HCT116 cells to ∼14%. Compared to MT, up to 30 and 36% increase in the cellular inhibition were recorded with MT + L + M and MT + MNP + L + M treatments, respectively, at 72 h culture. The differences in cell proliferation were marginal between MT + L + M and MT + MNP + L + M.

The results of similar proliferation assay experiments performed with HepG2 cells are shown in Figure 2f. It appears that the bare drug (MT) is relatively less effective in inhibiting HepG2 cells compared to HCT116 cells (Figure 2c) during the first 48 h of incubation, and at 72 h, both cells showed similar amounts of proliferation. The L + M treatment was found to aid HepG2 cell inhibition in the presence of MT (MT + L + M). However, after 72 h incubation, the maximum proliferation of HepG2 cells (40%, Figure 2f) could not match with HCT116 cells, which showed 20% under identical treatment conditions (Figure 2c). The MT + MNP + L + M treatment showed strong influence on HepG2 cells with 17% proliferation at the end of 72 h culture, and these cells showed relatively more inhibition during the first 48 h of culture compared to HCT116 cells.

2.3. Effect of LIPUS + SMF Treatment on Apoptosis and Cell Cycle. The results of cell-cycle analysis performed on two cancerous cell lines are presented in Figure 3. In both cell lines, the population of cells in the S phase increased in the presence of anticancer drug (MT) compared to the control group (Figure 3a,e), which is in line with the known blocking effect of MT drug.[51] The cell transition from the S to G_2 phase was found to be significantly reduced (>67% of cells in the S phase, $p < 0.05$ in Figure 3c) with MT + L + M treatment. No cells were observed in the G2 phase when HCT116 cells were treated with MT + MNP + L + M, as shown in Figure 3d. Cell-cycle analysis revealed that the HepG2 cells are more sensitive to L + M treatment, as shown in Figure 3g–h. With MT + L + M treatment, majority of the cells were restricted to the G1 phase, followed by the S phase (Figure 3g). Interestingly, 100% cell blockage to the G1 phase occurred in HepG2 cells with MT + MNP + L + M treatment. These observations demonstrate that the efficiency of MT and MT + MNP can be increased with LIPUS + SMF treatment, more effectively in HepG2 cells than in HCT116 cells.

The apoptosis assay of HCT116 shows 50% necrosis in the presence of MT (Figure 4b), which is significantly higher than that of control samples (20%, Figure 4a). However, Figure 4c shows that the cell response appears to be different when the MT was added in the presence of L + M treatment (MT + L + M), where a significant reduction in necrosis was observed. Moreover, the concentration of apoptotic cells was also increased to 29% from 6% in MT treatment (Figure 4b). Interestingly, when MT + MNP was administered along with L

DOI: 10.1021/acsomega.8b00105
ACS Omega 2018, 3, 5459−5469

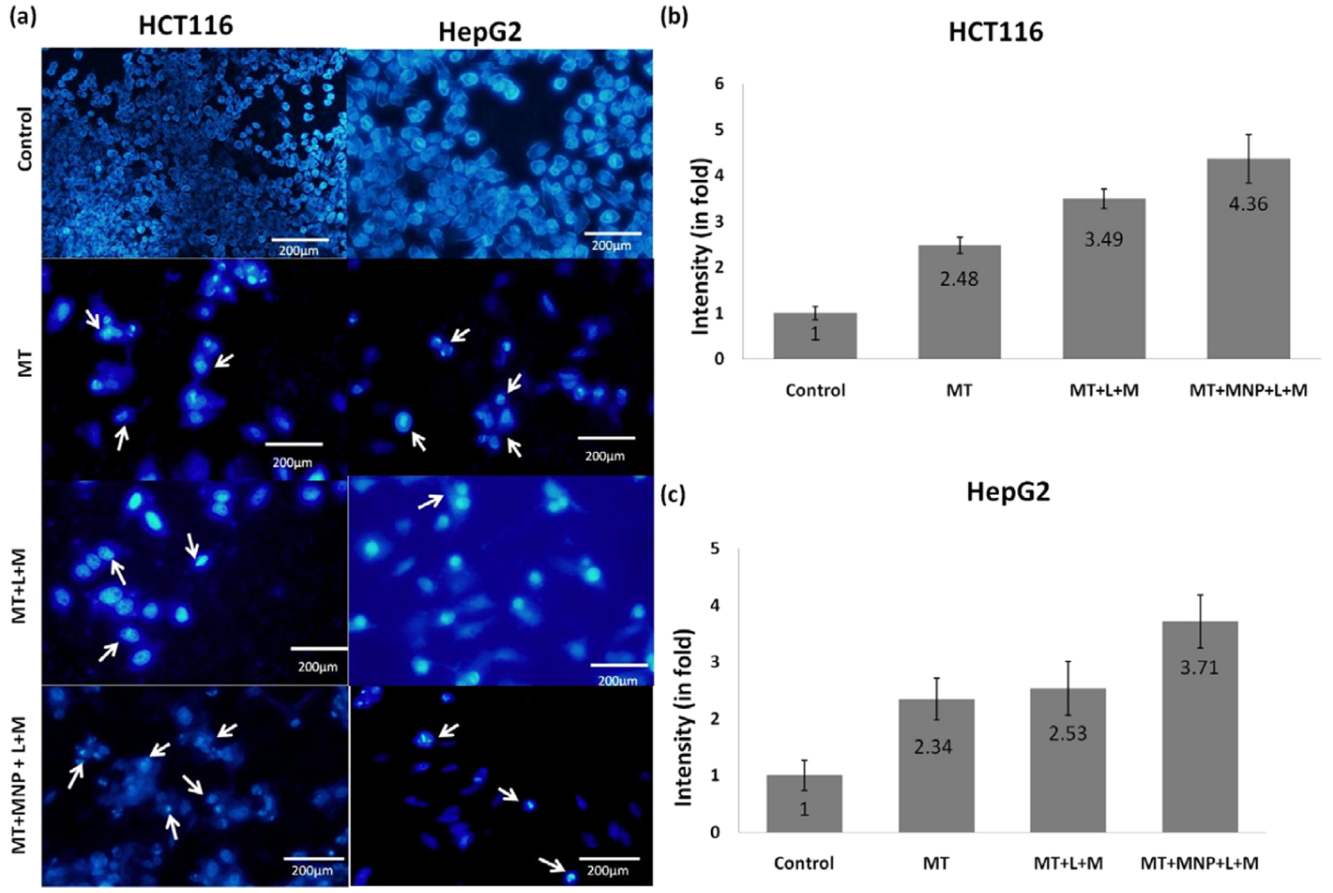

Figure 7. (a) Morphology of DAPI-stained HCT116 and HepG2 cell nuclei under different treatment conditions after 72 h incubation. The arrows indicate the cells with damaged cell nucleus. (b) Quantification of HCT116 cell damage in terms of nucleus intensity in fluorescence images. (c) Changes in the fluorescence nucleus intensity of HepG2 cells under different treatment conditions.

+ M treatment (Figure 4d), the apoptosis was further increased to 32%. The L + M treatment, with and without MNP, along with MT gradually increased the cellular transition from early to late apoptosis compared to bare MT. The response of HepG2 cells to these treatments was also found to be similar to HCT116 cells (Figure 4e–g). However, the amount of apoptotic and necrotic cells was high in HepG2 cells compared to HCT116 cells with MT + MNP + L + M treatment.

2.4. Intracellular ROS and Membrane Potential Changes. It is known that the oxidative stress, which is related to elevated intracellular levels of reactive oxygen species (ROS), can damage cell structure, DNA, proteins, and lipids, leading to cell death. Therefore, we have measured the oxidative stress generated under different treatment conditions in terms of ROS. As the ROS production can be directly related to the damage of the cellular structure, DNA, and proteins/lipids, the amount of ROS production in HCT116 and HepG2 cells was measured under different conditions. The results presented in Figure 5a indicate that the ROS intensity increased (164%) from 75 to 198 when the HCT116 cells were treated with MT and the intensity drastically increased to 695 with L + M treatment, almost 250% increase in the ROS production. Further increase in the intensity up to 763 was recorded with MT + MNP + L + M treatment. In case of HepG2 cells, the ROS intensity increased gradually from 491 for MT to about 1981 for MT + MNP + L + M treatment (Figure 5b). Compared to HCT116 cells, the MT + L + M and MT + MNP + L + M treatments resulted in 95 and 160% more ROS production in HepG2 cells, respectively.

The change in the cell membrane potential of HCT116 cells under different treatment conditions is shown in Figure 6a, where the peaks of treated cells shifted toward left, compared to the control group, indicating that they are hyperpolarized. Hyperpolarization can result in increased transmembrane transport of several ions, followed by cell death.[52−54] The severity of hyperpolarization was found to be maximum in HCT116 cells with MT + MNP + L + M treatment. HepG2 cells exhibited more gradual increase in the hyperpolarization with MT, MT + L + M, and MT + MNP + L + M treatment, as shown in Figure 6b. Maximum hyperpolarization was achieved with MT + MNP + L + M treatment, followed by MT + L + M and minimum with MT treatment.

2.5. Fluorescence Microscopy. The initiation of changes in the nucleus of HCT116 and HepG2 cells due to L + M treatment was observed using 4′,6-diamidino-2-phenylindole (DAPI) staining after 24 h culture. The morphology of DAPI-stained cell nuclei is presented in Figure 7a. It was observed that the MT-treated cells showed relatively more chromatin condensation in HCT116 cells compared to HepG2 cells, indicating better effect of anticancer drug on HCT116 in terms of apoptosis, as chromatin condensation is the primary indication of apoptosis. Chromatin condensation was prominent in both cells under MT + L + M treatment. Finally, the MT + MNP + L + M treatment appears to induce complete protein denaturization and nucleus damage in both HCT116

DOI: 10.1021/acsomega.8b00105
ACS Omega 2018, 3, 5459−5469

and HepG2 cells at 72 h incubation. The degree of nucleus damage was quantified by analyzing the nucleus intensity of fluorescence images using ImageJ software and compared with that of control group.[55] The results, shown in Figure 7b, revealed almost fourfold increase in the damage of HCT116 cells after MT + MNP + L + M treatment. Similarly, in HepG2 cells, the maximum cellular damage (3.71-fold) was achieved with MT + MNP + L + M treatment. The morphology and features of cell nucleus show damaged cell nucleus, which is an indication of apoptosis[56] that can directly induce cellular inhibition and thus provide overall improvement in the treatment efficacy.

2.6. Influence of LIPUS + SMF Treatment on Healthy Cells. The proposed L + M treatment was found to have a strong influence on cancer cell proliferation, as shown in Figure 2, but the potential negative effect of this treatment on normal/healthy cells is not known. Therefore, a similar cell proliferation assay was performed on MC3T3 (mouse pre-osteoblast) cells. The results (Figure 8) show that only LIPUS (L: 30 mW/cm^2) had very little inhibiting effect on the proliferation during the initial 24 h and the proliferation increased significantly after 48 and 72 h culture. The SMF (M: 150 mT) enhanced the cell proliferation at all culture durations. The L + M treatment had a maximum positive influence on MC3T3 cell proliferation, demonstrating its nontoxic effect on healthy cells.

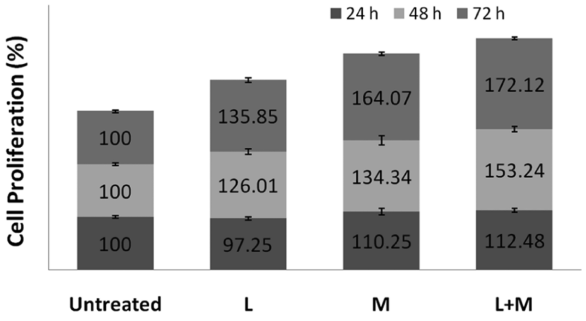

Figure 8. Proliferation of MC3T3 cells (n = 3) exposed to LIPUS (30 mW/cm^2) (L), SMF (150 mT) (M), and their combination (L + M) (p < 0.05 between untreated and treated samples).

3. DISCUSSION

In spite of significant research on DDS-based cancer treatment, its limitations, such as poor stability, reunion of nanosized DDS due to high surface area, limitation in target-site specificity for accumulation and delivery of effective biomolecules, high cost due to complex synthesis procedures, and poor invasiveness into tumor microenvironment, result in low treatment efficiency.[57−59] Therefore, newer adjuvant therapies that can enhance the overall efficiency of the current DDS are required. The present MT + MNP-based DDS with diffusion-controlled drug release at physiological pH shows acceptable conditions of release environment.[60] In this investigation, with the use of 30 mW/cm^2 LIPUS in the presence of 150 mT SMF (L + M), 15 min/day, the in vitro DDS inhibition effectiveness has been enhanced by 35% in colon (HCT 116) and hepatocellular (HepG2) carcinoma cells after 72 h incubation. The use of L + M treatment can generate a noninvasive synergy between the mechanical stress generated by LIPUS[61] and local electrical fields[22] generated by combinational exposure of LIPUS and SMF, which are believed to alter the activities of these cells by hyperpolarizing the cell membrane,[41] and production of large amounts of ROS resulting in observed cellular inhibition. As the cancer cells are known for their rapid proliferation assisted by their depolarized cellular membrane,[62] the LIPUS + SMF treatment-induced hyperpolarization destabilized the cell structure and increased the cellular apoptosis. The hyperpolarization of the cellular membrane results in an intra- and extracellular ionic imbalance of cancer cells via increased intake of anticancer drug (MT) or drug-loaded MNP (MT + MNP). Hyperpolarization via MT and MT + MNP internalization after exposure to LIPUS + SMF indicate a potential release of K^+ ions from cell interior or ingress of more Cl^- ions into the cells, leading to changes in the ionic gradient across the cell membrane. This imbalance of ionic flow changes the cell membrane permeability,[54] which directly leads to alteration of cellular conformation as well as restrict the DNA synthesis of cancer cells. Furthermore, the significantly high production of ROS in HepG2 cells compared to HCT116 cells clearly indicates that the treatment has varying influence depending on the cell type and therefore the treatment conditions must be optimized to treat different cancer types. The differences in treatment responses by different cells could be attributed to the variations in their characteristics, such as cell membrane potential.[63]

The cell-cycle restriction (blockage in the S phase or G1 → S phase transition) increased significantly due to the application of LIPUS + SMF in the presence of MT + MNP (no cells in the G_2 phase for HCT116 and no cells in the S and G_2 phases for HepG2). These results suggest that the L + M treatment creates hindrance in DNA synthesis, leading to cell-cycle arrest as a result of altered/destabilized cell membrane potential and enhanced intake of MT and MT + MNP by the cancer cells. Further, cell apoptosis analysis demonstrates that LIPUS + SMF treatment can accelerate the cellular activities of HCT116 and HepG2 cells, which is evinced by increase in the apoptotic cells (46% for HepG2 cells and 33% for HCT116 cells). A significant increase in the late apoptotic cell population of HepG2 cells (35%) also signifies loss of plasma membrane integrity and DNA fragmentation in these cells. Necrosis is caused by factors external to the cell or tissue, such as infection, toxins, or trauma, which result in the unregulated digestion of cell components. In contrast, apoptosis is a naturally occurring programmed and targeted cause of cellular death. One important finding in this analysis has been considerable reduction in necrosis of cells with L + M treatment. It is generally considered that necrosis is unprogrammed cell death and therefore detrimental to the biological system. Although late apoptotic and necrotic cells have permeabilized cell membranes, due to different events associated with their membrane damage, their response to clearance/removal signals would be different. Therefore, removal of necrotic cells from the system would be relatively more difficult than apoptotic cells.[64] The decrease in necrosis with L + M treatment is thus beneficial for cancer treatment with potentially low side effects. It is also evident that the synergetic effect of LIPUS + SMF treatment resulted in overproduction of ROS in both cell lines. The interaction of LIPUS + SMF treatment with polar and charged ionic elements of cells produced large amounts of ROS, which is a proinflammatory factor of cellular component responsible for cancer cell apoptosis.[22,56,65] Excessive production of ROS damages the DNA of cancer cells through the Fenton reaction[23] and results in oxidative stress accelerating apoptosis. It has been observed that the ion channels of cancer

DOI: 10.1021/acsomega.8b00105
ACS Omega 2018, 3, 5459−5469

cells are damaged leading to changes in their morphology and apoptosis due to excessive ROS production.[23]

We hypothesize that application of 30 mW/cm^2 LIPUS + 150 mT SMF can generate electrical and mechanical stimuli in situ during the treatment,[22,42] which are believed to be responsible for the observed enhancement in cancer cell inhibition with this treatment. Under present experimental conditions, the mechanical stimulus generated by LIPUS at the cell/soft tissue was estimated ($p = \sqrt{I \cdot Z}$, where p is the effective pressure (Pa), I is the intensity of ultrasound (W/cm^2), and Z is the acoustic impedance of the cell or soft tissue (kg/(m^2 s))) to be between 20 and 22 kPa. The estimated electrical field (E) ($E = \left(\frac{1}{C}\right) \cdot \left(\frac{p}{Z}\right) \cdot B$, where C is the velocity of light (m/s), B is the magnetic field strength (G); E is measured in electrostatic units esu (1 esu = 300 V/cm)) would be between 19 and 23 μV/cm. These in situ generated physical stimuli would have physically deformed (elastic or plastic) the cells/tissues, which can be seen from the hyperpolarization of the cell membranes. The intake of drug can be increased with the potential formation of stomas or lacunars in the cell membranes due to mechanical stress generated via LIPUS.[66−68] Moreover, the pressure induced by LIPUS has been demonstrated to induce ∼50 μm/s micromotions in the tissues,[69] which is believed to affect the membrane stability. As with externally applied electrical fields,[70] the in situ generated electrical fields, although small, would have negatively regulated the cancer cellular activities.[40] Interestingly, the L + M treatment was demonstrated to be safe for healthy cells (MC3T3) presumably due to differences in cell characteristics between cancer and healthy cells. However, toxicity due to the accumulation of these MNP is an important concern, which can be reduced by guiding the MNP using focused magnetic fields.[16] Another approach for targeting MNP with minimal accumulation involves functionalization of these NPs with tissue-specific adhesion molecules (homing receptors).[71,72] These two approaches are to be examined in conjunction with current LIPUS + SMF treatment to realize the full potential of this noninvasive treatment.

4. CONCLUSIONS

Detailed in vitro experimental results demonstrate that the proposed noninvasive LIPUS + SMF treatment can stimulate cancer cell inhibition three times better than bare drug or DDS. The treatment appears to be relatively more effective for early-time inhibition of HepG2 cells than HCT116 cells in the presence of MT + MNP. The production of ROS is also higher in HepG2 cells than in HCT116 cells. The treatment significantly reduced the amount of necrosis and induced hyperpolarization in both cancer cell lines. The in situ generated mechanical and electrical stimuli are thought to be responsible for the observed increase in cancer cellular inhibition via altered cell membrane characteristics. Since the treatment did not have any inhibitory effect on healthy cells, it is believed to have strong application potential to inhibit a variety of other cancer cell lines. The present in vitro results can form the basis for further investigations including targeting specific tissues, using homing molecule functionalized MNP and magnetic guidance, and in vivo trials to assess the effectiveness of this treatment.

5. MATERIALS AND METHODS

Deionized and decarbonized ultrapure water (Millipore, specific resistivity: 18 MΩ, conductivity: 0.05 μS/cm) was used in all preparations, and the chemicals used in this study were $Fe(NO_3)_3 \cdot 9H_2O$ (99.0%, Merck), NH_2OH (99.0%, Merck), urea (99.0%, Merck), NH_4OH (99.5%, Sigma-Aldrich), and methotrexate (99.5%, Sigma-Aldrich).

5.1. Synthesis and Characterization of MNP (α-Fe_2O_3)- and Methotrexate-Loaded MNP (MT + MNP). Fe_2O_3 nanoparticles (MNP) were synthesized following precipitation route using ammonia and urea. In a typical synthesis, 20 cc of ammonia solution (25%) was added dropwise to 20 cc of 0.1 M $Fe(NO_3)_3 \cdot 9H_2O$ solution at 90 °C and stirred for 1 h. A fine precipitate was obtained, which was filtered and washed three times with deionized water. Then, the water was removed with acetone (dehydrating agent), followed by overnight drying of the precipitate at 60 °C and calcination at 450 °C for 2 h. Since the primary focus of this investigation has been to evaluate the influence of LIPUS + SMF treatment on cancer cell inhibition, we have intentionally used weak ferromagnetic/paramagnetic nanoparticles to eliminate or reduce the accumulation of MNP during this treatment. Further, the use of magnetic field is to generate the proposed electrical field/charge noninvasively in the presence of LIPUS. In fact, in our earlier investigation, we have used nonmagnetic NPs to evaluate the influence of LIPUS + SMF treatment,[73] and in this investigation, we attempted to analyze the effect of magnetic carriers.

For anticancer drug loading, 1 g of calcined MNP was suspended in 5 cc of ethanol with 1 g of methotrexate (MT) and the solution was sonicated for 15 min. The prepared solution was aged overnight to evaporate the ethanol and obtain drug-loaded MNP (MT + MNP). For drug release study, 30 mg of MT + MNP was dispersed in 30 mL of freshly prepared PBS (pH 7.4) and was used as the analyte. Then, at specific time intervals, an aliquot of 3 mL was removed from the main stock and the optical density was determined using a UV−visible spectrophotometer (Lambda 35, PerkinElmer). Initially, a calibration curve was prepared to calculate the concentration of drug released into PBS at specific incubation time.

Powder X-ray diffraction (XRD) analysis of MNP was performed using an X'Pert Pro MPD diffractometer (PANalytical, Almelo, the Netherlands) in the 2θ range between 5 and 70°. The particle size of MNP and MT + MNP was measured by dynamic light scattering (Malvern, Germany) using dilute suspensions of powder in water. The ζ potential was determined using a Zetasizer (Zetasizer 2000, Malvern, Germany) with a dilute suspension of the powder in PBS having pH 7.4. The morphology of MNP and MT + MNP was studied using a transmission electron microscope (TECHNAI G2 30ST, and FEI). To identify the absorption bands of MT in MT + MNP, Fourier transform infrared (FTIR) spectra of the powder was recorded at room temperature using the KBr (Sigma-Aldrich, ≥99%) pellet method (sample: KBr = 1:100) using a spectrophotometer (Spectrum100, PerkinElmer) in the 400−4000 cm^{-1} range with an average of 50 scans. The magnetic properties of the powder (∼0.2 g) were determined using a vibrating sample magnetometer (VSM, LakeShore7407) under a maximum field of 15 kOe at room temperature. Thermogravimetric analyses (TGA)−differential thermal analysis (DTA) of the powder were carried out between 25 and 1000 °C at a heating rate of 10 °C/min in air to estimate the

DOI: 10.1021/acsomega.8b00105
ACS Omega 2018, 3, 5459−5469

absorption of MT on MNP using a TGA/DTA instrument (NETZSCH STA 409 CD, Germany).

5.2. Cytotoxicity Assay. *5.2.1. Cell Culture and IC_{50} of MT.* Human colon carcinoma (HCT116) and hepatocellular carcinoma (HepG2) (ATCC, Rockville, MD) cells were routinely cultured separately in Dulbecco's modified Eagle's medium (DMEM) (Invitrogen, Carlsbad) supplemented with 10% heat-inactivated fetal bovine serum, 1 U/mL penicillin G, and 1 mg/mL streptomycin, in a T_{75} flask in a CO_2 incubator (ESCO, Singapore) at 37 °C with 5% CO_2. It was distributed using a six-well plate after full confluency. The half-maximal inhibitory concentration (IC_{50}) of MT was evaluated at various concentrations in the range of 5−100 ng/mL with 10 mg/mL MT stock solution in dimethyl sulfoxide (DMSO, Sigma-Aldrich, India). After the cells were plated at 2×10^4/well density, they were incubated at 37 °C in a CO_2 incubator for 24 h to allow cell adhesion and the incubation was continued for a total duration of 72 h after the addition of MT ($n = 3$). After 72 h incubation, the MTT assay was performed by adding 10 μL of 3-(4,5-dimethylthiazole-2-yl)-2,5-phenyltetrazolium bromide (MTT) reagent with a concentration of 1 mg/mL (Sigma-Aldrich) in a 1:9 ratio (MTT/DMEM) to all wells and incubated in the dark for 4 h at 37 °C. Then, the solution was removed and 100 μL of DMSO was added to each well. The absorbance of the solution was measured at 550 nm in an ELISA reader (Bio-Rad) to generate the dose response curve. The IC_{50} was determined from the dose response curve.

5.2.2. Cell Proliferation Assay. Both HCT116 and HepG2 cells were subcultured in 35 mm Petri plates at a density of 2×10^4 and incubated overnight. Then, MT or MT + MNP was added at desired concentrations (MT at IC_{50} concentration for each cell line and MNP including MT at 46 μg/mL for HCT116 and 73 μg/mL for HepG2), followed by exposure to 3.5 and 150 mT SMF (⌀ 30 mm, 5−6 mm thick NdFeB permanent magnets) and LIPUS (probe ⌀ 22.22 mm, 30 mW/cm^2, 1.5 MHz, 200 μs pulse width at 1 kHz). The treatment (LIPUS + SMF) time was 15 min/day, and the MTT assay was performed after 24, 48, and 72 h incubation. A similar proliferation assay was also carried out using mouse pre-osteoblast cells (MC3T3) (ATCC, Rockville, MD) to assess the effect of LIPUS + SMF treatment on these healthy cells. The details of sample notations used in the present investigation are presented in Table 1.

5.3. Apoptosis and Cell-Cycle Analysis. To analyze the influence of different treatments on the cellular activities of HCT116 and HepG2 cells, cell-cycle analysis was performed using Cycletest PLUS DNA reagent kit (BD Cat no: 340242). The amount of cell apoptosis was determined by Annexin V/propidium iodide double-staining kit (BD Biosciences, Cat no: 556570). For the analysis, 1×10^5 treated cells were trypsinized and washed with 1× PBS and the suspended pellet was analyzed using a flow cytometer (CyFlow Cube 6, SysmexPartec GmbH, Germany). Both analyses were performed after 72 h culture duration.

5.4. Measurement of Reactive Oxygen Species (ROS) and Cell Membrane Potential. After desired treatment, the cells (1×10^5) were trypsinized, washed with 1× PBS, and resuspended in 1 mL of 1× PBS to detect ROS using standard detection assay kit (ab186029, Abcam, India). The intensity of 2′,7′-dichlorofluorescin diacetate was detected using a flow cytometer at 650 nm. Plasma membrane potential changes were measured using bis(1,3-dibutylbarbituric acid)-trimethineoxonol ($DiBAC_4(3)$ dye; Invitrogen, Carlsbad, CA). To measure the membrane potential, trypsinized cells were incubated in 100 nM $DiBAC_4(3)$ dye for 10 min in the dark and then the mean fluorescence intensity was measured using a flow cytometer at 488 nm.

5.5. Fluorescence Microscopy. Qualitative analysis of treated cancer cells in terms of their nucleus and nuclear membrane structures was carried out by DAPI (Cat no: D1306, Thermo Fisher) staining. The cells were plated at a density of 3×10^3 in a 35 mm Petri plate. After desired culture duration (72 h), the cells were rinsed with PBS three times, followed by fixing for 10 min in 3.7% formaldehyde. The cells were permeabilized by immersing in 0.2% Triton X-100 for 5 min and incubating the cells for 1−5 min at room temperature in diluted DAPI solution (1:5000). After aspirating the labeled solution, the cells were rinsed three times in PBS. Counter-staining was performed by adding 2.5 μg/mL fluorescein isothiocyanate to each well and kept for 5 min and then washed three times using PBS. Finally, the cells were imaged using a fluorescence microscope (Olympus BX51TRF, Tokyo, Japan).

5.6. Statistical Analysis. The data obtained in cell proliferation, cell apoptosis, cell cycle, ROS, and membrane potential measurements were statistically analyzed using the Student t-test and $p < 0.05$ was considered statistically significant.

Table 1. Sample Notations and Treatment Conditions Used for Cell Proliferation Analysis Using MTT Assay

sample ID	treatment conditions
control	only cells were cultured
untreated	treated with either anticancer drug (MTX) or drug-delivery system (MT + MNP), but no exposure of external stimuli, i.e., no SMF and/or LIPUS treatment.
MT	treated with MTX
MT + MNP	treated with MT + MNP
M	treated with SMF (3.5 or 150 mT)
L	treated with LIPUS (30 mW/cm^2)
L + M	treated with SMF + LIPUS
MT + L + M	treated with anticancer drug and SMF + LIPUS
MT + MNP + L + M	treated with drug-delivery system (MT + MNP) and SMF + LIPUS

AUTHOR INFORMATION

Corresponding Author

*E-mail: vamsiballa@cgcri.res.in. Tel: 033-2429 4179. Fax: 033-2473 0957.

ORCID

Vamsi K. Balla: 0000-0003-2796-7302

Notes

The authors declare no competing financial interest.

ACKNOWLEDGMENTS

The authors acknowledge financial support from the Council of Scientific and Industrial Research (CSIR), India, under grants ESC 0103 and SRF fellowship to S.S.

REFERENCES

(1) Brahimi-Horn, M. C.; Chiche, J.; Pouysségur, J. Hypoxia and Cancer. *J. Mol. Med.* **2007**, *85*, 1301−1307.

(2) Brown, J. M. Tumor Hypoxia in Cancer Therapy. *Methods Enzymol.* **2007**, *435*, 297−321.

DOI: 10.1021/acsomega.8b00105
ACS Omega 2018, 3, 5459−5469

(3) Harada, H. How Can We Overcome Tumor Hypoxia in Radiation Therapy. *J. Radiat. Res.* **2011**, *52*, 545−556.
(4) Avni, R.; Cohen, B.; Neeman, M. Hypoxic Stress and Cancer: Imaging the Axis of Evil in Tumor Metastasis. *NMR. Biomed.* **2011**, *24*, 569−581.
(5) Felfoul, O.; Mohammadi, M.; Taherkhani, S.; De Lanauze, D.; Zhong Xu, Y.; Loghin, D.; Essa, S.; Jancik, S.; Houle, D.; Lafleur, M.; Gaboury, L.; Tabrizian, M.; Kaou, N.; Atkin, M.; Vuong, T.; Batist, G.; Beauchemin, N.; Radzioch, D.; Martel, S. Magneto-Aerotactic Bacteria Deliver Drug-Containing Nanoliposomes to Tumour Hypoxic Regions. *Nat. Nanotechnol.* **2016**, *11*, 941−947.
(6) Eisenbrey, J. R.; Shraim, R.; Liu, J.-B.; Li, J.; Stanczak, M.; Oeffinger, B.; Leeper, D. B.; Keith, S. W.; Jablonowski, L. J.; Forsberg, F.; O'Kane, P.; Wheatley, M. A. Sensitization of Hypoxic Tumors to Radiation Therapy Using Ultrasound-Sensitive Oxygen Microbubbles. *Int. J. Radiat. Oncol., Biol., Phys.* **2018**, 88−96.
(7) Chertok, B.; David, A. E.; Yang, V. C. Brain Tumor Targeting of Magnetic Nanoparticles for Potential Drug Delivery: Effect of Administration Route and Magnetic Field Topography. *J. Controlled Release* **2011**, *155*, 393−399.
(8) Chertok, B.; Moffat, B. A.; David, A. E.; Yu, F.; Bergemann, C.; Ross, B. D.; Yang, V. C. Iron Oxide Nanoparticles as a Drug Delivery Vehicle for MRI Monitored Magnetic Targeting of Brain Tumors. *Biomaterials* **2008**, *29*, 487−496.
(9) Wahajuddin; Arora, S. Superparamagnetic Iron Oxide Nanoparticles: Magnetic Nanoplatforms as Drug Carriers. *Int. J. Nanomed.* **2012**, *7*, 3445−3471.
(10) Sengupta, S.; Sasisekharan, R. Exploiting Nanotechnology to Target Cancer. *Br. J. Cancer* **2007**, *96*, 1315−1319.
(11) Hergt, R.; Dutz, S. Magnetic Particle Hyperthermia-Biophysical Limitations of a Visionary Tumour Therapy. *J. Magn. Magn. Mater.* **2007**, *311*, 187−192.
(12) Etheridge, M. L. Understanding the Benefits and Limitations of Magnetic Nanoparticle Heating for Improved Applications in Cancer Hyperthermia and Biomaterial Cryopreservation. Ph.D. Thesis, University of Minnesota, 2013.
(13) Jarockyte, G.; Daugelaite, E.; Stasys, M.; Statkute, U.; Poderys, V.; Tseng, T. C.; Hsu, S. H.; Karabanovas, V.; Rotomskis, R. Accumulation and Toxicity of Superparamagnetic Iron Oxide Nanoparticles in Cells and Experimental Animals. *Int. J. Mol. Sci.* **2016**, *17*, 1193.
(14) Johannsen, M.; Gneveckow, U.; Thiesen, B.; Taymoorian, K.; Cho, C. H.; Waldöfner, N.; Scholz, R.; Jordan, A.; Loening, S. A.; Wust, P. Thermotherapy of Prostate Cancer Using Magnetic Nanoparticles: Feasibility, Imaging, and Three-Dimensional Temperature Distribution. *Eur. Urol.* **2007**, *52*, 1653−1662.
(15) Whittow, G. C. The Effect of Hyperthermia on the Systemic and Pulmonary Circulation of the Ox (*Bos taurus*). *Q. J. Exp. Physiol. Cogn. Med. Sci.* **1965**, *50*, 300−311.
(16) Estelrich, J.; Escribano, E.; Queralt, J.; Busquets, M. A. Iron Oxide Nanoparticles for Magnetically-Guided and Magnetically-Responsive Drug Delivery. *Int. J. Mol. Sci.* **2015**, *16*, 8070−8101.
(17) Cameron, I.; Short, N.; Markov, M. Safe Alternative Cancer Therapy Using Electromagnetic Fields. *Environmentalist* **2007**, *27*, 453−456.
(18) de Seze, R.; Tuffet, S.; Moreau, J. M.; Veyret, B. Effects of 100 mT Time Varying Magnetic Fields on the Growth of Tumors in Mice. *Bioelectromagnetics* **2000**, *21*, 107−111.
(19) Tofani, S.; Barone, D.; Cintorino, M.; de Santi, M. M.; Ferrara, A.; Orlassino, R.; Ossola, P.; Peroglio, F.; Rolfo, K.; Ronchetto, F. Static and ELF Magnetic Fields Induce Tumor Growth Inhibition and Apoptosis. *Bioelectromagnetics* **2001**, *22*, 419−428.
(20) Tofani, S.; Cintorino, M.; Barone, D.; Berardelli, M.; De Santi, M. M.; Ferrara, A.; Orlassino, R.; Ossola, P.; Rolfo, K.; Ronchetto, F.; Tripodi, S. A.; Tosi, P. Increased Mouse Survival, Tumor Growth Inhibition and Decreased Immunoreactive p53 after Exposure to Magnetic Fields. *Bioelectromagnetics* **2002**, *23*, 230−238.
(21) Ghodbane, S.; Lahbib, A.; Sakly, M.; Abdelmelek, H. Bioeffects of Static Magnetic Fields: Oxidative Stress, Genotoxic Effects, and Cancer Studies. *BioMed. Res. Int.* **2013**, *2013*, No. 602987.
(22) Montalibet, A.; Jossinet, J.; Matias, A.; Cathignol, D. Electric Current Generated by Ultrasonically Induced Lorentz Force in Biological Media. *Med. Biol. Eng. Comput.* **2001**, *39*, 15−20.
(23) Berk, M.; Dodd, S.; Henry, M. Do Ambient Electromagnetic Fields Affect Behaviour? A Demonstration of the Relationship between Geomagnetic Storm Activity and Suicide. *Bioelectromagnetics* **2006**, *27*, 151−155.
(24) Rattner, D. W. Future Directions in Innovative Minimally Invasive Surgery. *Lancet* **1999**, *353*, S112−S115.
(25) Chen, W.-F.; Qi, H.; Sun, R.-G.; Liu, Y.; Zhang, K.; Liu, J.-Q. Static Magnetic Fields Enhanced the Potency of Cisplatin on K562 Cells. *Cancer Biother. Radiopharm.* **2010**, *25*, 401−408.
(26) Liu, Y.; Qi, H.; Sun, R.-G.; Chen, W.-F. An Investigation into the Combined Effect of Static Magnetic Fields and Different Anticancer Drugs on K562 Cell Membranes. *Tumori* **2011**, *97*, 386−392.
(27) Gourevich, D.; Hertzberg, Y.; Volovick, A.; Shafran, Y.; Navon, G.; Cochran, S.; Melzer, A. Ultrasound-Mediated Targeted Drug Delivery Generated by Multifocal Beam Patterns: An in Vitro Study. *Ultrasound Med. Biol.* **2013**, *39*, 507−514.
(28) Feril, L. B., Jr.; Kondo, T.; Cui, Z.-G.; Tabuchi, Y.; Zhao, Q.-L.; Ando, H.; Misaki, T.; Yoshikawa, H.; Umemura, S. Apoptosis Induced by the Sonomechanical Effects of Low Intensity Pulsed Ultrasound in a Human Leukemia Cell Line. *Cancer Lett.* **2005**, *221*, 145−152.
(29) Jiang, Z.; Wu, W.; Qian, M. Cellular Damage and Apoptosis along with Changes in NF-Kappa B Expression Were Induced with Contrast Agent Enhanced Ultrasound in Gastric Cancer Cells and Hepatoma Cells. *Cancer Cell Int.* **2012**, *12*, 8.
(30) Hirokawa, N.; Koito, K.; Okada, F.; Kudo, N.; Yamamoto, K.; Fujimoto, K.; Nishida, M.; Ichimura, T.; Hori, M.; Satoh, T.; Hareyama, M. High-Intensity Focused Ultrasound Induced Apoptosis with Caspase 3, 8, and 9/6 Activation in Rat Hepatoma. *J. Ultrason. Med.* **2009**, *36*, 177.
(31) Miller, D. L.; Dou, C. Induction of Apoptosis in Sonoporation and Ultrasonic Gene Transfer. *Ultrasound Med. Biol.* **2009**, *35*, 144−154.
(32) Liu, Y.; Kon, T.; Li, C.; Zhong, P. High Intensity Focused Ultrasound-Induced Gene Activation in Sublethally Injured Tumor Cells in Vitro. *J. Acoust. Soc. Am.* **2005**, *118*, 3328−3336.
(33) Harada, Y.; Ogawa, K.; Irie, Y.; Endo, H.; Feril, L. B.; Uemura, T.; Tachibana, K. Ultrasound Activation of TiO_2 in Melanoma Tumors. *J. Controlled Release* **2011**, *149*, 190−195.
(34) Buldakov, M. A.; Feril, L. B.; Tachibana, K.; Cherdyntseva, N. V.; Kondo, T. Low-Intensity Pulsed Ultrasound Enhances Cell Killing Induced by X-Irradiation. *Ultrason. Sonochem.* **2014**, *21*, 40−42.
(35) Borasi, G.; Melzer, A.; Russo, G.; Nahum, A.; Zhang, Q.; Alongi, F.; Vicari, F.; Gilardi, M. C. Cancer Therapy Combining High-Intensity Focused Ultrasound and Megavoltage Radiation. *Int. J. Radiat. Oncol., Biol., Phys.* **2014**, *89*, 926−927.
(36) Eisenbrey, J. R.; Huang, P.; Hsu, J.; Wheatley, M. A. Ultrasound Triggered Cell Death in Vitro with Doxorubicin Loaded Poly Lactic-Acid Contrast Agents. *Ultrasonics* **2009**, *49*, 628−633.
(37) Guan, L.; Xu, G. Damage Effect of High-Intensity Focused Ultrasound on Breast Cancer Tissues and Their Vascularities. *World J. Surg. Oncol.* **2016**, *14*, 153.
(38) Choijamts, B.; Naganuma, Y.; Nakajima, K.; Kawarabayashi, T.; Miyamoto, S.; Tachibana, K.; Emoto, M. Metronomic Irinotecan Chemotherapy Combined with Ultrasound Irradiation for a Human Uterine Sarcoma Xenograft. *Cancer Sci.* **2011**, *102*, 452−459.
(39) Kondo, T.; Yoshida, T.; Ogawa, R.; Hassan, M. A.; Furusawa, Y.; Zhao, Q.-L.; Watanabe, A.; Morii, A.; Feril, L. B., Jr.; Tachibana, K.; Kitagawa, H.; Tabuchi, Y.; Takasaki, I.; Shehata, M. H.; Kudo, N.; Tsukada, K. Low-Intensity Ultrasound Adjuvant Therapy: Enhancement of Doxorubicin-Induced Cytotoxicity and the Acoustic Mechanisms Involved. *J. Med. Ultrason.* **2009**, *36*, 61−68.

DOI: 10.1021/acsomega.8b00105
ACS Omega 2018, 3, 5459−5469

(40) McCaig, C. D.; Rajnicek, A. M.; Song, B.; Zhao, M. Controlling Cell Behavior Electrically: Current Views and Future Potential. *Physiol. Rev.* **2005**, *85*, 943−978.
(41) Napotnik, T. B.; Reberšek, M.; Vernier, P. T.; Mali, B.; Miklavčič, D. Effects of High Voltage Nanosecond Electric Pulses on Eucaryotic Cells (in Vitro): A Systematic Review. *Bioelectrochemistry* **2016**, *110*, 1−12.
(42) Nuccitelli, R.; Pliquett, U.; Chen, X.; Ford, W.; James Swanson, R.; Beebe, S. J.; Kolb, J. F.; Schoenbach, K. H. Nanosecond Pulsed Electric Fields Cause Melanomas to Self-Destruct. *Biochem. Biophys. Res. Commun.* **2006**, *343*, 351−360.
(43) Giladi, M.; Weinberg, U.; Schneiderman, R. S.; Porat, Y.; Munster, M.; Voloshin, T.; Blatt, R.; Cahal, S.; Itzhaki, A.; Onn, A.; Kirson, E. D.; Palti, Y. Alternating Electric Fields (Tumor-Treating Fields Therapy) Can Improve Chemotherapy Treatment Efficacy in Non-Small Cell Lung Cancer Both in Vitro and in Vivo. *Semin. Oncol.* **2014**, *41*, S35−S41.
(44) Nuccitelli, R.; Wood, R.; Kreis, M.; Athos, B.; Huynh, J.; Lui, K.; Nuccitelli, P.; Epstein, E. H. First-in-Human Trial of Nano-electroablation Therapy for Basal Cell Carcinoma: Proof of Method. *Exp. Dermatol.* **2014**, *23*, 135−137.
(45) Meng Lin, M.; Kim, H.-H.; Kim, H.; Muhammed, M.; Kim, D. K. Iron Oxide-Based Nanomagnets in Nanomedicine: Fabrication and Applications. *Nano Res.* **2010**, *1*, 4883.
(46) Divakaran, S. A.; Sreekanth, K. M.; Rao, K. V.; Nair, C. K. K. D-Aminoacid Oxidase-Fe_2O_3 Nanoparticle Complex Mediated Anti-tumor Activity in Swiss Albino Mice. *J. Cancer Ther.* **2011**, *2*, 666−674.
(47) Li, Y.; Zhu, C.; Kan, J. Preparation and Characteristics of γ-Fe_2O_3/Polyaniline-Curcumin Composites. *Metals* **2015**, *5*, 2401−2412.
(48) Qu, J.; Liu, G.; Wang, Y.; Hong, R. Preparation of Fe_3O_4-Chitosan Nanoparticles Used for Hyperthermia. *Adv. Powder Technol.* **2010**, *21*, 461−467.
(49) Mahdavi, M.; Ahmad, M.; Haron, M.; Namvar, F.; Nadi, B.; Rahman, M.; Amin, J. Synthesis, Surface Modification and Characterisation of Biocompatible Magnetic Iron Oxide Nanoparticles for Biomedical Applications. *Molecules* **2013**, *18*, 7533−7548.
(50) Chakraborty, M.; Dasgupta, S.; Sengupta, S.; Chakraborty, J.; Ghosh, S.; Ghosh, J.; Mitra, M. K.; Mishra, A.; Mandal, T. K.; Basu, D. A Facile Synthetic Strategy for Mg−Al Layered Double Hydroxide Material as Nanocarrier for Methotrexate. *Ceram. Int.* **2012**, *38*, 941−949.
(51) Savage, J. R. K.; Prasad, R. Generalized Blocking in S Phase by Methotrexate. *Mutat. Res.* **1988**, *201*, 195−201.
(52) Li, S.-D.; Huang, L. Reviews Pharmacokinetics and Biodistribution of Nanoparticles. *Mol. Pharmaceutics* **2008**, *5*, 496−504.
(53) Soto-Cerrato, V.; Manuel-Manresa, P.; Hernando, E.; Calabuig-Fariñas, S.; Martínez-Romero, A.; Fernández-Dueñas, V.; Sahlholm, K.; Knöpfel, T.; García-Valverde, M.; Rodilla, A. M.; Jantus-Lewintre, E.; Farrás, R.; Ciruela, F.; Pérez-Tomás, R.; Quesada, R. Facilitated Anion Transport Induces Hyperpolarization of the Cell Membrane That Triggers Differentiation and Cell Death in Cancer Stem Cells. *J. Am. Chem. Soc.* **2015**, *137*, 15892−15898.
(54) Yang, M.; Brackenbury, W. Membrane Potential and Cancer Progression. *Front. Physiol.* **2013**, *4*, 185.
(55) Gerlitz, G.; Bustin, M. Efficient Cell Migration Requires Global Chromatin Condensation. *J. Cell Sci.* **2010**, *123*, 2207−2217.
(56) Okkenhaug, K.; Bilancio, A.; Emery, J. L.; Vanhaesebroeck, B. Phosphoinositide 3-Kinase in T Cell Activation and Survival. *Biochem. Soc. Trans.* **2004**, *32*, 332−335.
(57) Naseri, N.; Valizadeh, H.; Zakeri-Milani, P. Solid Lipid Nanoparticles and Nanostructured Lipid Carriers: Structure, Preparation and Application. *Adv. Pharm. Bull.* **2015**, *5*, 305−313.
(58) Madaan, K.; Kumar, S.; Poonia, N.; Lather, V.; Pandita, D. Dendrimers in Drug Delivery and Targeting: Drug-Dendrimer Interactions and Toxicity Issues. *J. Pharm. BioAllied Sci.* **2014**, *6*, 139−150.
(59) Wahajuddin; Arora, S. Superparamagnetic Iron Oxide Nanoparticles: Magnetic Nanoplatforms as Drug Carriers. *Int. J. Nanomed.* **2012**, *7*, 3445−3471.
(60) Dash, S.; Murthy, P. N.; Nath, L.; Chowdhury, P. Kinetic Modeling on Drug Release from Controlled Drug Delivery Systems. *Acta Pol. Pharm.* **2010**, *67*, 217−223.
(61) Hoffman, B. D.; Grashoff, C.; Schwartz, M. A. Dynamic Molecular Processes Mediate Cellular Mechanotransduction. *Nature* **2011**, *475*, 316−323.
(62) Hanahan, D.; Weinberg, R. A. Hallmarks of Cancer: The next Generation. *Cell* **2011**, *144*, 646−674.
(63) Gillet, J.-P.; Varma, S.; Gottesman, M. M. The Clinical Relevance of Cancer Cell Lines. *J. Natl. Cancer Inst.* **2013**, *105*, 452−458.
(64) Poon, I. K. H.; Hulett, M. D.; Parish, C. R. Molecular Mechanisms of Late Apoptotic/necrotic Cell Clearance. *Cell. Death Differ.* **2010**, *17*, 381.
(65) Ozben, T. Oxidative Stress and Apoptosis: Impact on Cancer Therapy. *J. Pharm. Sci.* **2007**, *96*, 2181−2196.
(66) Mo, S.; Coussios, C. C.; Seymour, L.; Carlisle, R. Ultrasound-Enhanced Drug Delivery for Cancer. *Expert Opin. Drug Delivery* **2012**, *9*, 1525−1538.
(67) Tachibana, K.; Uchida, T.; Ogawa, K.; Yamashita, N.; Tamura, K. Induction of Cell-Membrane Porosity by Ultrasound. *Lancet* **1999**, *353*, 1409.
(68) Baker, K. G.; Robertson, V. J.; Duck, F. A. A Review of Therapeutic Ultrasound: Biophysical Effects. *Phys. Ther.* **2001**, *81*, 1351−1358.
(69) Bolander, M. E.; Greenleaf, J. F.; Bronk, J. T.; Kinnick, R. R. Generation of Micromotion in Soft Tissue Adjacent to Fractured Bone by Pulsed Ultrasound-Generated Pressure Waves. *Bone* **2005**, *36*, S192−S193.
(70) Ghibelli, L.; Cerella, C.; Cordisco, S.; Clavarino, G.; Marazzi, S.; De Nicola, M.; Nuccitelli, S.; D'Alessio, M.; Magrini, A.; Bergamaschi, A.; Guerrisi, V.; Porfiri, L. M. NMR Exposure Sensitizes Tumor Cells to Apoptosis. *Apoptosis* **2006**, *11*, 359−365.
(71) Sackstein, R.; Schatton, T.; Barthel, S. R. T-lymphocyte homing: an underappreciated yet critical hurdle for successful cancer immunotherapy. *Lab. Invest.* **2017**, *97*, 669−697.
(72) Ager, A.; Watson, H. A.; Wehenkel, S. C.; Mohammed, R. N. Homing to solid cancers: a vascular checkpoint in adoptive cell therapy using CAR T-cells. *Biochem. Soc. Trans.* **2016**, *44*, 377−385.
(73) Sengupta, S.; Khatua, C.; Jana, A.; Balla, V. K. Use of Ultrasound with Magnetic Field for Enhanced in Vitro Drug Delivery in Colon Cancer Treatment. *J. Mater. Res.* **2018**, 625−637.

DOI: 10.1021/acsomega.8b00105
ACS Omega 2018, 3, 5459−5469